PLANETARY SCIENCE

Titan's spin state as a constraint on tidal dissipation

Brynna G. Downey[1,2]* and Francis Nimmo[2]

Tidal dissipation in satellites affects their orbital and rotational evolution and their ability to maintain subsurface oceans. However, a satellite's dissipation rate, parameterized by k_2/Q, is hard to measure and is only known for the Moon and Io. Here, we use Titan's measured departure from its expected rotation state to infer k_2/Q and its boundary layer dissipation parameter K/C_s. Over the likely range of ocean and ice shell thicknesses, we infer a K/C_s of 6.3×10^{-14} s^{-1} to 2.4×10^{-10} s^{-1}, a k_2/Q of 0.058 to 0.12, and a minimum dissipation factor $Q \approx 5$. Titan's dissipation parameters are one to two orders of magnitude larger than the Moon's and suggest an interior with a low effective viscosity. Titan's dissipation rate implies that its eccentricity and inclination are damping rapidly, consistent with an excitation within the last ~350 Myr. The forthcoming Dragonfly lander could measure Titan's tidal response, and JUICE could use our approach to determine Ganymede's k_2/Q.

INTRODUCTION

Satellites experience tides raised by their planets, and the rate at which tidal energy is dissipated inside the satellite depends on the factor k_2/Q (*1*, *2*). The Love number k_2 describes how deformable the body is to tides, and the quality factor Q is related to the lag in the body's tidal response to the primary's gravitational force (a smaller Q means a greater lag, which means more dissipation) (*3*). Tidal dissipation in the satellite controls how rapidly its orbit shrinks, circularizes, and becomes planar (*1*). Measurements of k_2 and k_2/Q also help with inferences about the satellite's interior structure, such as whether it contains a subsurface ocean (*4*, *5*). However, despite its importance in understanding a satellite's orbital evolution and interior, k_2/Q is hard to measure.

The Moon and Io are the only two satellites with a measured k_2/Q. For the Moon, k_2/Q has been determined using a combination of laser ranging and spacecraft tracking (*6*) and for Io, k_2/Q comes from astrometry (*7*) and spacecraft tracking (*5*). The Cassini spacecraft performed over 100 flybys of Titan, collecting data on Titan's gravitational field and rotational state (*8*, *9*). Notably, Cassini radio science measured $k_2 = 0.62$ for Titan, making it only the second satellite after the Moon whose tidal response has been measured (*4*, *10*). However, existing studies either derived bounds on k_2/Q that were consistent with zero (*10*, *11*) or did not solve for it (*12*). We use existing measurements of Titan's rotation state to infer the value of k_2/Q, concluding that Titan experiences a high rate of tidal dissipation at the present day.

Our approach uses the measured angular offset in Titan's spin axis to quantify energy dissipation. The equilibrium spin axis orientation of a satellite is called a Cassini state after G.D. Cassini documented characteristics of the spin state of the Moon (*13*). In a Cassini state, the spin axis and orbit normal both precess about the normal to the Laplace plane (defined as the average orbital plane) at the same rate and with the same or opposite phase (*13*, *14*). The geometry of this configuration is such that during the precession cycle, all three vectors lie in the same plane, which we refer to as the Cassini plane. In the presence of dissipative torques, Cassini states are the expected termini of spin evolution (*15*–*19*).

Although dissipation brings the system toward equilibrium, it also causes the end spin state to be offset from the Cassini plane, meaning that the planar configuration is never quite reached (*20*, *21*). The magnitude of a body's Cassini plane offset is connected to the total amount of dissipation in the interior, including tidal dissipation. The only bodies in the solar system that are confirmed to be in a Cassini state are the Moon (*20*–*22*), Titan (*8*, *23*), and Mercury (*24*, *25*), and all three have nonzero Cassini plane offsets. Fits to the lunar laser ranging (LLR) data are able to distinguish between two distinct sources of dissipation in the Moon: tides and differential rotation between the solid mantle and fluid core (*18*). In the Supplementary Materials, we show that while Titan is expected to experience differential rotation between the solid ice shell and ocean, in most combinations of ice shell and ocean thickness, tides are likely the dominant source of dissipation today.

The rest of this manuscript is organized as follows: We first present an analytical expression for the Cassini plane offset as a function of tidal and fluid-solid boundary dissipation. We corroborate our expression with observations of the Moon's Cassini plane offset. We next apply the theory to determine Titan's k_2/Q, which, to our knowledge, has not been done before and discuss the implications for its tidal-orbital history. We end with implications for other satellites in our solar system, including Io and Ganymede.

RESULTS

Equilibrium Cassini plane offset with tidal and boundary layer dissipation

In equilibrium, the spin axis of a synchronous satellite is configured so as to balance the torques acting on its outer solid layer, which is the mantle for the Moon and the ice shell for Titan. We consider three torques on a general outer solid layer: the gravitational torque exerted by the planet on the satellite's permanent triaxial figure, the torque on its tidal bulge, and the torque resulting from differential rotation at the fluid-solid boundary. This boundary is the core-mantle boundary (CMB) for the Moon and the ocean-ice shell boundary for Titan. Tidal dissipation depends on the factor k_2/Q, where the tidal Love number k_2 measures the magnitude of the body's tidal response and $1/Q$ is related to its phase lag relative to the imposed potential. Dissipation at the fluid-solid boundary depends on the factor K/C_s, where K is the viscous dissipation parameter and C_s is the general polar moment of inertia of the outer solid layer. The viscous dissipation

[1]Southwest Research Institute, Boulder, CO 80302, USA. [2]Department of Earth and Planetary Sciences, University of California Santa Cruz, Santa Cruz CA 95064, USA. *Corresponding author. Email: brynna.downey@swri.org

parameter K is defined and calculated in the Supplementary Materials. For the Moon, C_s is the moment of inertia of the mantle C_m, and for Titan, C_s is the moment of inertia of the ice shell C_{sh}.

In the reference frame of a uniformly precessing orbit, the spin axis unit vector is $\boldsymbol{s} = (s_x, s_y, s_z) = (\sin\theta\cos\phi, \sin\theta\sin\phi, \cos\theta)$. The obliquity θ is the angle between the spin axis and orbit normal $\boldsymbol{n}$, and ϕ is the azimuth in the orbit plane measured from the positive x axis (see Fig. 1). In this geometry, the Cassini plane formed by the orbit normal $\boldsymbol{n}$ and the Laplace plane normal $\boldsymbol{k}$ is the xz plane. The orbital inclination i is the angle between $\boldsymbol{n}$ and $\boldsymbol{k}$.

Without dissipation, $\boldsymbol{s}$ precesses about $\boldsymbol{k}$ with the same or opposite phase as $\boldsymbol{n}$, so it lies in the Cassini plane. With dissipation, $\boldsymbol{s}$ is out of phase in the precession cycle compared to $\boldsymbol{n}$ but has the same frequency, so it maintains a small yet constant offset from the Cassini plane. The spin axis $\boldsymbol{s}$ is separated from the Cassini plane by a distance s_y, an angle γ, which is the Cassini plane offset, and an azimuth shift of Δϕ (Fig. 1). The relations are that $s_y = \sin\theta \sin\phi$, $|s_y| = |\sin\gamma|$, and to determine whether γ is a positive phase lag or a negative phase lead, $\sin\gamma = \sin\theta \sin\Delta\phi$ (see the Supplementary Materials).

We derive the magnitude of the equilibrium Cassini plane offset γ (see Materials and Methods) as a function of the tidal dissipation factor k_2/Q and the boundary layer dissipation factor K/C_s assuming synchronous rotation and only a single forcing frequency (that of the orbit precession)

$$|\sin\gamma| = \left[3\frac{k_2}{Q}\frac{n}{c}\frac{M_p}{M}\left(\frac{R}{a}\right)^3\left(1-\frac{1}{2}\cos\theta\right)\sin\theta + \frac{K}{C_s}\sin\Delta\epsilon\right]\frac{\sin\theta}{|\dot{\Omega}\sin i|} \quad (1)$$

where M_p is the mass of the planet and R, M, c, n, a, i, and $\dot{\Omega}$ are the satellite's radius, mass, normalized polar moment of inertia for the whole body ($C = cMR^2$), orbital mean motion, semimajor axis, inclination between the orbit and Laplace plane, and retrograde precession frequency of the orbit about the Laplace plane, respectively. The angle between the outer solid and fluid spin axes is Δε, which factors in viscous and pressure coupling at the fluid-solid boundary (see the Supplementary Materials). Our Eq. 1 can be related to the expression for the Cassini plane offset in (*26*) (see Materials and Methods).

In the absence of dissipation (i.e., $k_2/Q = K/C_s = 0$), $\gamma = 0$, so $\boldsymbol{s}$ lies in the Cassini plane. With dissipation, γ is nonzero, so $\boldsymbol{s}$ lies off the Cassini plane. Equation 1 is the key expression for this paper, because it relates the observable quantity γ to dissipation factors that are otherwise hard to measure.

Verifying our approach with the moon

LLR data have detected a Cassini plane offset of $\gamma = -7.5 \times 10^{-5}$° for the Moon (*18*, *20*, *22*). In addition to tidal heating, the Moon experiences friction at the CMB because the spin axis of the fluid core is expected to align with the ecliptic normal rather than with the mantle spin axis (*20*, *27*).

The lunar Cassini plane offset can be connected to both tides and differential rotation via Eq. 1. Because there are two potential sources of dissipation, Fig. 2 shows the set of nonunique solutions of k_2/Q and K/C_m that produce the same offset. There are two end-member scenarios: one in which tides account for the full offset, where $k_2/Q = 1.2 \times 10^{-3}$, and one in which friction at the CMB does, where $K/C_m = 4.1 \times 10^{-13}$ s^{-1}.

Fits to the LLR data are able to discern between dissipation due to tides and differential rotation because they damp the free libration modes and the orbital elements differently (*18*). From LLR data

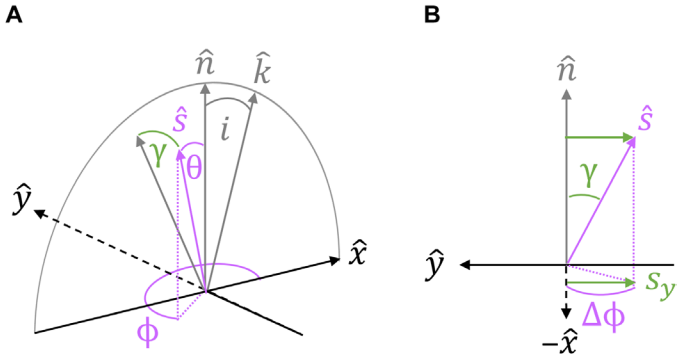

Fig. 1. Cassini plane offset geometry for Cassini state 1. (**A**) Skewed perspective of the Cassini plane (**B**) side-on view of the Cassini plane. The Cassini plane is the xz plane formed by the orbit normal $\boldsymbol{n}$ and the Laplace plane normal $\boldsymbol{k}$. Everything in gray lies in the Cassini plane. With dissipation, the y component of the spin axis s_y, the azimuth relative to the Cassini plane Δϕ, and the Cassini plane offset γ are nonzero. The relations are $|s_y| = |\sin\theta \sin\Delta\phi| = |\sin\gamma|$.

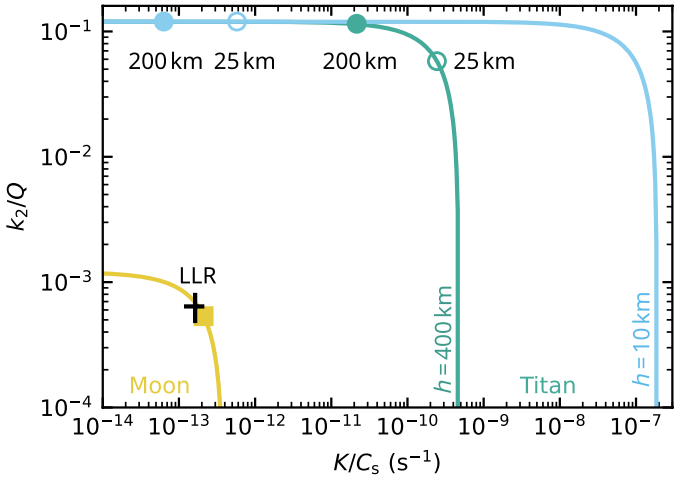

Fig. 2. Titan's dissipation parameters are orders of magnitude larger than the Moon's. The curves are the theoretical dissipation parameters that produce the Cassini plane offsets of the Moon (yellow) and Titan (green/blue), using Eq. 1. Tidal dissipation is parameterized by k_2/Q and friction at the solid-fluid boundary by K/C_s. For the Moon, we present the parameters and their error bars fit to the LLR data (*6*) (cross) along with our calculated values (yellow square) (see the Supplementary Materials). Titan's green curve is for an ocean thickness $h = 400$ km, and the blue for $h = 10$ km. Titan's filled dots are for an ice shell thickness $d = 200$ km, and empty dots for $d = 25$ km. The four dots mark our lower and upper bounds for d and h, and they produce a range of K/C_s of 6.3×10^{-14} s^{-1} to 2.4×10^{-10} s^{-1}. The k_2/Q for each point is that needed to produce the remainder of the Cassini plane offset not produced by a particular K/C_s. The range of k_2/Q is 0.058 to 0.12.

analyses, $k_2/Q = (6.4 \pm 1.5) \times 10^{-4}$ and $K/C_m = (1.63 \pm 0.39) \times 10^{-13}$ s^{-1} (*6*), so about half of the lunar Cassini plane offset can be attributed to solid-body tides and half to differential rotation at the CMB. Our solution curve in Fig. 2 matches very well with the LLR parameters.

We follow the methodology in (*18*) and independently find that $K/C_m = 2.1 \times 10^{-13}$ s^{-1} (see the Supplementary Materials). Factoring in viscous and pressure coupling, we corroborate that the angle of separation between the core and mantle spin axes is $\Delta\varepsilon = 1.63$° (*28*, *29*) instead of $\Delta\varepsilon = 1.543$° as assumed by LLR analyses (see the Supplementary Materials). For $K/C_m = 2.1 \times 10^{-13}$ s^{-1} and $\Delta\varepsilon = 1.63$°,

the remainder of γ yields $k_2/Q = 5.4 \times 10^{-4}$, so our solution is within error of the LLR solution. Having thus validated our approach, we now apply our methodology to Titan.

Application to Titan

Analyses of Cassini radar images found Titan's spin state, consisting of θ = 0.323° and γ = 0.091° (*8*) and more recently θ = 0.31° (*30*). Factoring in uncertainties in the International Astronomical Union (IAU) orbit determination, (*23*) obtained θ = 0.32 ± 0.02° and γ = 0.12 ± 0.02°, which we will use here [see discussion in (*31*)]. Titan's ocean spin axis will not be aligned perfectly with that of the ice shell, so we consider both tides and differential rotation at the ocean-ice shell boundary to explain Titan's Cassini plane offset.

For Titan, we provide a range of likely K/C_{sh} and their corresponding k_2/Q because the end-member differential rotation scenarios depend on the unknown angular separation between the ocean and ice shell spin axes Δε. The value for Δε depends in turn on the degree of pressure coupling which is affected by the unknown ice shell and ocean thicknesses, d and h (see the Supplementary Materials). For d = 25 to 200 km and h = 10 to 400 km, we calculate the ranges $\Delta\varepsilon = 1.6 \times 10^{-4}$ to 0.065° and $K/C_{sh} = 6.3 \times 10^{-14}$ to 2.4×10^{-10} s^{-1}. The complementary range for k_2/Q is 0.058 to 0.12. Figure 2 shows how the lower and upper bounds of d and h relate to the bounds on K/C_{sh} and k_2/Q. In general, a smaller h means smaller Δε, which produces smaller K/C_{sh} (compare the green and blue dots). A smaller d means a smaller C_{sh} and greater turbulent dissipation in the boundary layer, so larger K (compare the filled and empty dots). Details on the methodology for calculating K/C_{sh} and Δε are in the Supplementary Materials.

Titan's tidal end-member is $k_2/Q = 0.12 \pm 0.027$. The smallest value $k_2/Q = 0.058$ is for h = 400 km and d = 25 km, and a thicker ice shell or a thinner ocean raises k_2/Q closer toward the tidal end-member scenario (Fig. 2). We did not explore smaller d because the calculations produced K/C_{sh} values larger than the theoretical end-members and so did not represent a self-consistent combination of parameters. The uncertainty on the end-member k_2/Q comes from the uncertainty in the obliquity and Cassini plane offset (*23*) and the normalized polar moment of inertia (see the Supplementary Materials).

Our results are consistent with some interior models and with the upper bounds from gravity data. Adding dissipation to their tidal analysis, (*10*) found that Titan's time-variable gravity coefficients are compatible with $k_2/Q < 0.2$ (including zero) and $k_2 = 0.62$. Interior models for Titan with low viscosities can also produce $k_2/Q < 0.1$ and $k_2 = 1.0$ (*4*).

A caveat is that we neglect the second instance of differential rotation, that between the ocean and the solid interior below it. We neglect atmospheric effects on the ice shell (*32*). We neglect tidal dissipation in the subsurface ocean (*33*–*37*) because this represents work done by the tidal potential (*35*). If there is a net torque that the solid core, atmosphere, or ocean flow exerts on the ice shell on the other hand, then this would contribute to the Cassini plane offset. In any event, the large k_2/Q values that we have derived here indicate a large source of dissipation located somewhere within Titan.

Dynamical implications for Titan

Our inferred range of k_2/Q of 0.058 to 0.12 would produce substantial tidal heating in Titan. The standard rates of solid-body tidal heating in a synchronous satellite for small eccentricity e and obliquity θ are $\dot{E}_e$ and $\dot{E}_\theta$, respectively (*2*, *38*)

$$\{\dot{E}_e, \dot{E}_\theta\} = \frac{3}{2}\frac{k_2}{Q}\frac{n^5 R^5}{G}\{7e^2, \sin^2\theta\} \quad (2)$$

Energy dissipation from differential rotation at the fluid-solid boundary is less important, but we include it for completeness (*18*)

$$\dot{E}_f = K\,|\Delta\omega|^2 \quad (3)$$

Figure 3A shows the heating from solid-body eccentricity and obliquity tides as a function of k_2/Q. For comparison, the heating from ocean obliquity tides is 1.4×10^{-6} Wm^{-2} using the scaling laws in (*36*) and a bottom drag coefficient $c_D = 2.4 \times 10^{-6}$ from the Reynolds number scaling law in (*39*). The present-day radiogenic heat estimate for Titan is 3×10^{-3} W m^{-2} (*40*, *41*).

The points on Fig. 3A are the same four cases shown in Fig. 2 to capture the lower and upper bounds on ice shell thickness d and ocean thickness h. The tidal end-member k_2/Q of 0.12 would produce

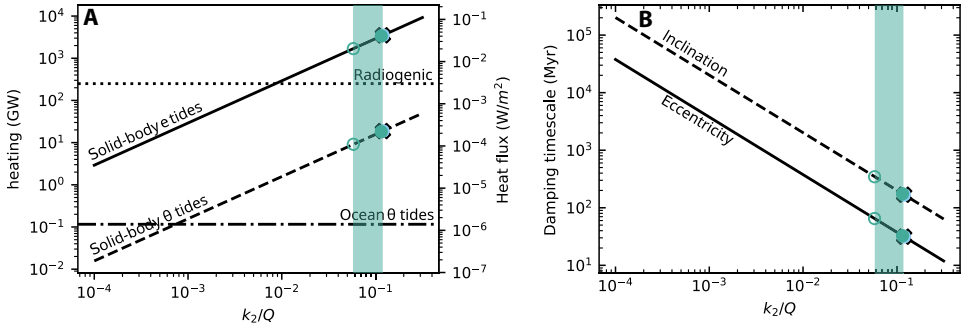

Fig. 3. Titan's strong solid-body tidal heating suggests a recent source of its eccentricity and inclination. (**A**) Titan's heating as a function of k_2/Q for solid-body eccentricity tides (solid), solid-body obliquity tides (dashed), ocean obliquity tides [dash-dot (*36*)], and radiogenic heating [dotted, (*40*, *41*)]. The black crosses mark the values for the tidal end-member k_2/Q = 0.012. The four colored dots are the same cases as in Fig. 2 and represent the minimum and maximum d and h that we consider. The range of k_2/Q that these edge cases suggest is 0.058 to 0.12 (green shaded region) with a heat flux range of 20 to 42 mW m^{-2}. The dots along the solid-body obliquity tide line also include boundary layer friction, which is a negligible 10^3 to 6×10^7 W. (**B**) How Titan's eccentricity and inclination damping timescales depend on k_2/Q. The dashed line is the inclination damping timescale from solid-body obliquity tides alone, but the dots also include boundary layer friction. For the maximum k_2/Q = 0.12, the damping timescales are τ_e ~ 30 Myr and τ_i ~ 170 Myr, and for a minimum k_2/Q = 0.058, τ_e ~ 65 Myr and τ_i ~ 350 Myr. All of these timescales, in particular the eccentricity damping timescale, are much shorter than the age of the solar system.

a surface heat flux of 42 mW m^{-2}, primarily due to solid-body eccentricity tides, which is an order of magnitude higher than the present-day radiogenic heating. The lower bound on k_2/Q of 0.058 would produce a surface heat flux of 20 mW m^{-2}.

Energy dissipation in Titan causes its semimajor axis to shrink at a rate (*42*)

$$\frac{da}{dt} = -\frac{2a^2}{GM_pM}\dot{E}_{\text{tot}} \quad (4)$$

where $\dot{E}_{\text{tot}}$ is the total energy dissipation which includes solid-body eccentricity and obliquity tides (Eq. 2) and turbulent friction at the ocean-ice shell boundary (Eq. 3).

The inferred k_2/Q range would contribute a semimajor axis shrinking rate of −3 to −6 cm/year (Eq. 4). From astrometry, Titan's observed semimajor axis expansion rate is +11 cm/year (*11*), although this is fit dependent (*12*). Titan's fast semimajor axis expansion rate is driven by tidal dissipation in Saturn, and assuming no tidal dissipation in Titan, Saturn's Q ~ 100 at Titan's orbital frequency (*11*). If the Q of Titan is as low as we suspect, then to produce the same semimajor axis change of +11 cm/year, the Q of Saturn at Titan's orbital frequency is even lower than ~100.

A natural question is whether Titan's orbital elements could survive damping due to tidal heating over the lifetime of the solar system (*33*, *34*, *43*–*45*). The rate of eccentricity and inclination decay due to energy extracted from the orbit, e.g., satellite eccentricity and obliquity tides, is (*42*)

$$\frac{de}{dt} = -\frac{a}{GM_pM}\frac{1-e^2}{e}\dot{E}_e \quad (5)$$

$$\frac{di}{dt} = -\frac{a}{GM_pM}\frac{1}{\tan i}\dot{E}_\theta \quad (6)$$

Using Eqs. 5 and 6, we calculate an order of magnitude damping timescale for the eccentricity $\tau_e = e/de/dt$ and inclination $\tau_i = \tan i/di/dt$. For $k_2/Q = 0.12$, τ_e ~ 30 Myr and τ_i ~ 170 Myr. For $k_2/Q = 0.058$, τ_e ~ 65 Myr and τ_i ~ 350 Myr. Turbulent friction at the fluid-solid boundary lowers the inclination and shrinks the semimajor axis but is an order of magnitude less effective at doing so than tides (*18*). Because the differential rotation in this case is rooted in misaligned spin axes for the ice shell and ocean, which does not depend on eccentricity, the turbulent dissipation does not change the eccentricity. Figure 3B shows the eccentricity and inclination damping timescales as a function of k_2/Q. The solid-body k_2/Q would have to be ≤0.001 ($Q \geq 600$) for the eccentricity damping timescale to be the age of the solar system and ≤ 0.006 ($Q \geq 100$) for the inclination damping timescale to be the age of the solar system. The tidal damping timescales of Titan's orbital elements are much shorter than the age of the solar system, suggesting a recent excitation (see Discussion).

Interior implications for Titan

If Titan's ice shell is conductive, our maximum inferred surface heat flux of 42 mW m^{-2} (about 3.5 TW) suggests a relatively low equilibrium ice shell thickness, $d \approx 20$ km if heating occurs below the ice shell, or somewhat thicker if the heating is in the ice shell (*46*). Such a thickness is lower than the 55 to 80 km inferred from a detection of a Schumann-like resonance in Titan's atmosphere (*47*) and the ~100 km from topography analyses (*46*). For a convecting ice shell, a heat flux of 42 mWm^{-2} is at the high end of existing model estimates (*41*, *48*) but would permit a thicker ice shell.

Our minimum inferred tidal heat flux of 20 mW m^{-2} (about 2 TW) yields an equilibrium ice shell thickness of $d \approx 100$ km if tidal and radiogenic heating occurs below the shell. However, this heat flux was derived assuming that $d = 25$ km (Fig. 3A); the internal contradiction suggests that the higher k_2/Q and heat flux values discussed above are more likely.

There are no constraints that our findings can place on the values of h and the flattening of the ocean-ice shell boundary. What we can say is that both h and the ocean flattening affect the alignment of the ocean and ice shell spin axes. For increased flattening or a smaller h, the ocean and ice shell spin axes will be more aligned (see the Supplementary Materials), which will decrease K, and imply a larger k_2/Q and surface heat flux.

Titan's degree-2 potential Love number from Cassini data is $k_2 = 0.616 \pm 0.067$ (*4*, *10*), so taking an upper bound within error of $k_2/Q < 0.147$, the tidal quality factor, Q, has a lower bound of $Q \geq 3.7$. Another analysis of Cassini radiometric tracking data found k_2 in the range 0.3 to 0.4 (*49*), implying a lower bound on Q of 2.0 to 2.7.

We can ask what solid-body viscosity would be required to yield the inferred lag in Titan's tidal response k_2/Q. Using the expression in (*4*), $k_2/Q = 0.12$ would require an effective viscosity of the whole body of 3×10^{13} Pa s, which is on the lower end of the range of estimates for high-pressure ice, 10^{12} to 10^{23} Pa s (*50*). In a simple Titan model, in which we reduce the viscosities of the solid core and high-pressure ice layers of (*51*) to an ice-like value of 10^{15} Pa s, we obtain a Q of 10. Neither of these calculations is meant to be a realistic model but simply to emphasize that our understanding of Titan's internal structure is not currently good enough to be able to rule out a Q of 5 on theoretical grounds.

Titan's low Q value is lower than previous assumptions but comparable to the Q of some other solar system bodies at their respective tidal frequencies. From astrometric observations of the change in semimajor axis and eccentricity (*7*) paired with spacecraft tracking during Galileo and Juno flybys, Io's $k_2/Q = 0.0109 \pm 0.0054$, in which case $Q = 11.4 \pm 3.6$ (*5*). The Earth's Q is ~13 (*1*, *52*), mostly due to dissipation in the shallow surface ocean. Primarily solid-body Q's are larger: that for Mars is ~90 (*53*) and for the Moon which has $k_2/Q = 6.4 \times 10^{-4}$ and $k_2 = 0.024$, $Q = 38$ at monthly periods (*6*).

Application to Io, Europa, Ganymede, and Callisto

Io's Cassini plane offset has never been observed, but heat flow measurements, astrometry, and spacecraft tracking indicate that it has a solid-body k_2/Q of 0.0109 (*5*, *7*). Doing the reverse analysis as for the Moon and Titan, we predict the Cassini plane offset to be at least 1.5×10^{-5}° (Table 1).

The upcoming Europa Clipper mission aims to determine Europa's rotation state, including its obliquity and librations. As yet, the precision with which the spin state will be determined from imaging and a rotational ephemeris is unavailable. To get a 0.004 accuracy in the moment of inertia, (*54*) state a desire to have 0.05 arcmin (8.3×10^{-4}°) accuracy in the obliquity. If this accuracy were to apply to the Cassini plane offset as well, a $k_2/Q > 0.02$ would be detectable.

Ganymede's spin state has been observed (*55*), but its obliquity has not been determined nor are there any direct measurements of its k_2/Q. The upcoming ESA JUICE mission will have the capability to measure the orientation of Ganymede's spin axis (*56*) and thus

derive k_2/Q independent of time-variable gravity measurements. The obliquity is projected to have an uncertainty of 1 μrad or 5.7×10^{-5}° (*56*), which if applicable to the whole spin axis, means a signature of $k_2/Q > 1.6 \times 10^{-3}$ should be detectable in the Cassini plane offset. The tidal heat flux for $k_2/Q = 1.6 \times 10^{-3}$ would be a negligible ~0.1 mW m^{-2}.

JUICE is also expected to retrieve the spin state of Callisto from 21 flybys, although with an accuracy of only 5.5 mrad for the obliquity (*57*). Callisto's obliquity, let alone Cassini plane offset, will not be well constrained since the predicted obliquity from Eq. 9 is 0.13°, while the accuracy is 0.32°. The obliquity may be larger than expected either due to a subsurface ocean or due to resonant perturbations as may be the case for Titan (*23*).

Table 1 contains the observed spin angles for the Moon and Titan, their end-member k_2/Q and K/C, and the predicted spin angles for Io, Europa, and Ganymede from either measured or detectable k_2/Q. We assume that, like Titan, Europa's and Ganymede's ice shells will be aligned with the spin axes of their subsurface oceans, so we only predict the tidal endmembers. For Io, we neglect the effect of a possible magma ocean on the spin state of the crust. Table 2 contains the physical and dynamical parameters used to calculate the spin angles in Table 1.

DISCUSSION

We have argued that a sufficiently precise measurement of a satellite's offset from a Cassini state can be used to infer the rate of tidal dissipation from Eq. 1. Any torque that produces energy dissipation would contribute to the Cassini plane offset, but here we only consider the tidal torque and differential rotation torque at a fluid-solid boundary. Other works incorporate more sources, for example, (*26*) also explores viscoelastic deformation of the possible lunar solid inner core and (*29*) explores dissipation at the lunar inner core boundary. Other complicating factors at Titan that we have neglected are atmospheric torques (*58*, *59*), a pressure torque from the ocean acting on the ice shell, and the gravitational effect of the solid interior on the ice shell (*23*, *31*, *59*).

We have also neglected any net torque from ocean tides. If tidal dissipation in Titan's subsurface ocean does exert a net torque on the ice shell, then it could account for some of the Cassini plane offset. For example, if Titan's ocean happens to be resonantly stratified, up to about 1 TW of the maximum total tidal dissipation of ~3.5 TW could be due to ocean eccentricity tidal dissipation (*37*). Only ~10^8 W could be from equilibrium ocean obliquity tides. Given the number of potential sources of deformation and torques, further analysis to disentangle their effects on the Cassini plane offset would be desirable.

A limitation of our rotational model is that we can only explain Titan's Cassini plane offset and not its obliquity. Titan's obliquity from Cassini radar images (0.32°) is ~3× larger than expected (0.10°) from the Cassini state relation (Eqs. 9 and 15). Put another way, the spin axis precesses about the Laplace plane normal at about half the rate it should [687 years (*12*) given that it is in a Cassini state versus 346 years calculated from its obliquity and gravity measurements]. It was suggested by (*60*) that Titan's larger obliquity is from the ice shell being mechanically decoupled from the interior by a subsurface ocean. In the same vein, a proposed mechanism is that the presence of an ocean introduces free modes in the system that resonantly amplify Titan's obliquity (*23*, *31*). The models in (*23*, *31*) can explain Titan's obliquity but not its Cassini plane offset. In contrast, we attempt to explain Titan's Cassini plane offset, while taking the obliquity as a

Table 1. Spin angles and endmember dissipative parameters for several satellites. All values that have been measured directly are denoted with an asterisk (*), and the rest are predicted. The cross (+) indicates the minimum value that could be detected by spacecraft missions.

	θ (°)	Δϕ (°)	γ (°)	k_2/Q end-member	K/C (s^{-1}) end-member
Moon	6.67*	-6.5×10^{-4}*	-7.5×10^{-5}*	0.0012	4.0×10^{-13}
Titan	0.32*	22*	0.12*	0.12	4.7×10^{-10}–1.9×10^{-7}
Io	0.0022	0.38	1.5×10^{-5}	0.0109*	-
Europa	0.054	0.86	8.1×10^{-4}+	0.02	-
Ganymede	0.035	0.096	5.8×10^{-5}+	0.0016	-

Table 2. Physical and orbital parameters for satellites studied here. Unless specified otherwise, values are from JPL SSD Database. The Moon's J_2 and C_{22} are from GRAIL (*71*); the Moon's c is from GRAIL and LLR (*22*); Titan's J_2, C_{22}, and c are from Cassini (*10*); Io's J_2, C_{22}, and c are from Galileo (*72*); and Ganymede's J_2, C_{22}, and c are from Galileo and Juno (*73*). The nodal precessions for Io and Ganymede are from (*74*).

	M_p (kg)	M (kg)	R (km)	a (km)	e	i (°)	$2\pi/\dot{\Omega}$ (year)	J_2	C_{22}	c
Moon	5.97×10^{24}	7.3×10^{22}	1738.0	0.38×10^6	0.055	5.16	18.6	203.3×10^{-6}	22.4×10^{-6}	0.393
Titan	5.68×10^{26}	13.5×10^{22}	2575.5	1.22×10^6	0.029	0.28	687.4	33.1×10^{-6}	10.4×10^{-6}	0.341
Io	1.90×10^{27}	8.9×10^{22}	1821.5	0.42×10^6	0.005	0.04	7.4	1845.9×10^{-6}	553.7×10^{-6}	0.377
Ganymede	1.90×10^{27}	14.8×10^{22}	2631.2	1.07×10^6	0.001	0.21	136.1	133.0×10^{-6}	39.6×10^{-6}	0.316

given. If we had assumed a lower value for Titan's obliquity, either its rigid-body value or that expected for the solid core (see the Supplementary Materials), we would have derived a higher k_2/Q (see Eq. 1). Further work should simultaneously solve for both the obliquity and the Cassini plane offset.

With $k_2/Q < 0.12$, Titan has a minimum eccentricity and inclination damping timescale of 30 and 170 Myr, which is consistent with a recent excitation of Titan's present-day orbital elements. Titan's present-day eccentricity of $e = 0.029$ is hard to explain if it is a relic of a larger primordial value that has damped due to tidal heating over the lifetime of the solar system (*33*, *34*, *43*–*45*). Several mechanisms to increase Titan's eccentricity have been suggested including its formation from several giant impacts (*61*), accretion of the mid-sized Saturnian satellites in the last 100 Myr (*62*), a near-resonance between Jupiter and Saturn (*63*), and recent close encounters with a lost satellite or with collisional debris (*62*, *64*–*66*).

A future orbiter to Titan should be able to measure k_2/Q directly from time-variable gravity (*67*). Combining this measurement with ours would then allow a direct determination of the magnitude of differential rotation or atmospheric torques (Fig. 2) and place constraints on Titan's ocean characteristics. More immediately, the upcoming Dragonfly mission to Titan will be able to detect the tidal deformation of the crust via surface measurements (*68*). The time lag between when the tidal deformation occurs and when Saturn is directly overhead is related to Q. For a minimum Q of 5 and an orbital period of 15.9 days, the tidal time lag will be $\Delta t = 1/nQ \approx 43{,}700$ s or about 12 hours. Such a lag should be detectable, providing a future test for the k_2/Q derived here.

MATERIALS AND METHODS

In this work, we relate dissipative torques in a body to the magnitude of the Cassini plane offset following the approaches of (*19*) and (*18*). Many other authors have investigated Cassini state dynamics, and a noncomprehensive list of useful references includes (*14*, *15*, *17*, *26*, *31*).

Spin dynamics without dissipation

A satellite's spin axis precesses about its orbit normal because of torques that the planet exerts on its permanent triaxial figure. At the same time, the satellite's orbit plane precesses due to torques from the planet's oblateness, the Sun, and other perturbing bodies such as neighboring satellites. The satellite's average orbit plane, the Laplace plane, lies between the primary's equator and orbit planes. Assuming uniform precession at one frequency, the orbit normal precesses about the Laplace plane normal at a rate (*13*, *69*)

$$\frac{d\boldsymbol{n}}{dt} = \dot{\Omega}(\boldsymbol{n}\times\boldsymbol{k}) \tag{7}$$

where $\boldsymbol{n}$ is the orbit normal, $\boldsymbol{k}$ is the normal to the Laplace plane, and $\dot{\Omega}$ is the precession of the longitude of the ascending node of the orbit plane on the Laplace plane.

In the reference frame of the precessing orbit with $\boldsymbol{n}$ along the z axis, the orbit-averaged rate of change of the spin axis of a triaxial solid body in a circular orbit is (*13*, *69*)

$$\left.\frac{d\boldsymbol{s}}{dt}\right|_{\text{rot}} = \frac{3}{2}\frac{n^2}{c\omega}\left[\left(J_2+C_{22}\right)(\boldsymbol{s}\cdot\boldsymbol{n})+C_{22}\right](\boldsymbol{s}\times\boldsymbol{n}) + \dot{\Omega}(\boldsymbol{s}\times\boldsymbol{k}) \tag{8}$$

where $\boldsymbol{s}$ is the spin axis unit vector, J_2 and C_{22} are the degree-2 gravity coefficients, c is the normalized polar moment of inertia of the whole body, n is the orbital mean motion, and ω is the spin angular velocity.

We define $\boldsymbol{n} = (0, 0, 1)$, $\boldsymbol{s} = \left(s_x, s_y, s_z\right) = (\sin\theta\cos\phi, \sin\theta\sin\phi, \cos\theta)$, and $\boldsymbol{k} = (\sin i, 0, \cos i)$. The obliquity θ is the angle between the spin axis and orbit normal, ϕ is the longitude of the ascending node of the equator plane on the orbit plane as measured from the positive y axis, and i is the inclination of the orbit to the Laplace plane (see Fig. 1). Because the orbit precesses about the Laplace plane, the spin axis's net motion is also to precess about the Laplace plane. It is convenient to set up the spin geometry in this way because nonzero values of ϕ are diagnostic of dissipation in the satellite, whereas θ is usually weakly affected and so cannot be used alone to quantify the total amount of dissipation.

The system occupies what is known as a Cassini state (*13*) when the spin axis and orbit normal have the same period of precession about the Laplace plane normal, which can only happen for specific values of the obliquity. In the absence of tidal dissipation, the Cassini state obliquity satisfies the following relation, which results from the steady-state solution to the y component of Eq. 8 (*14*, *69*)

$$\frac{3}{2}\frac{n^2}{c\omega}\left[\left(J_2+C_{22}\right)\cos\theta+C_{22}\right]\sin\theta = \mp\dot{\Omega}\sin(i\pm\theta) \tag{9}$$

Similarly, a requirement for $ds_x/dt = ds_z/dt = 0$ is that $s_y = 0$, which means that $\phi = 0$ or π and all motion is constrained to the xz plane. A common convention has $\theta > 0$ along the positive x axis and $\theta < 0$ along the negative x axis, which we seek to avoid in favor of having θ always be positive. Since θ is always positive, the top signs in Eq. 9 are for Cassini state 1, and the bottom signs are for Cassini state 2 (see the Supplementary Materials for more information on when a body is in Cassini state 1 versus 2).

There are several caveats with our simple treatment of the spin equations of motion of the outer solid layer of a body. We do not include terms for the pressure coupling between the ocean and ice shell or the gravitational force of the interior of the body on the outer solid layer. These are only included when determining the angular separation between the fluid and outer solid spin axes (Supplementary Materials). These effects act to align the obliquities of the ice shell, ocean, and solid interior. Neglecting pressure and gravitational coupling for Titan's ice shell is justified if its layers are aligned and Titan acts like a rigid body. As we show in the Supplementary Materials, Titan's ocean spin axis is <0.065° away from the spin axis of the ice shell. We do not know, however, the orientation of Titan's solid interior and whether it is aligned with the rest of the body. Since the solid interior certainly has a larger polar moment of inertia than the ice shell, to have the same Cassini state precession, it needs a smaller obliquity (ignoring resonant amplification). Titan's ice shell may be approximately aligned with the ocean but probably not with the solid interior. Either way, Titan's obliquity is not that of a rigid body (*23*, *69*). In the end, this work does not try to explain Titan's obliquity, only the Cassini plane offset, so dissipation is the most important effect to constrain.

Spin dynamics with tidal dissipation

Tidal torques drive the satellite to an equilibrium end point, which is usually a Cassini state and a spin angular velocity commensurate with the orbital mean motion. Past works have developed various ways to include tidal torques on the spin axis evolution (*15*–*17*, *19*, *26*, *70*). The tidal torque averaged over one orbit period is (*15*, *17*, *19*)

$$\boldsymbol{\tau}_{\mathbf{T}} = C\omega T\left[-\frac{1}{2}\boldsymbol{s}+\left(\frac{n}{\omega}-\frac{1}{2}\cos\theta\right)\boldsymbol{n}\right] \tag{10}$$

Where $C = cMR^2$ is the satellite's polar moment of inertia and T is a parameter defined as (*17*, *19*)

$$T = 3\frac{k_2}{Q}\frac{n}{c}\left(\frac{M_p}{M}\right)\left(\frac{R}{a}\right)^3 \tag{11}$$

where M and R are the satellite's mass and radius, and k_2/Q is the tidal dissipation parameter. From here on out, we deal only with synchronous satellites (i.e., $\omega = n$), which allows us to approximate the time lag between when the planet is overhead and when the satellite's tidal bulge responds as $\Delta t = 1/nQ$.

It is convenient to define a unit vector $\boldsymbol{e}$ that lies in the equator plane, perpendicular to both $\boldsymbol{s}$ and the line of nodes, and pointing toward $\boldsymbol{n}$ such that $\boldsymbol{n} = \cos\theta\boldsymbol{s} + \sin\theta\boldsymbol{e}$, and $\boldsymbol{e} = (\boldsymbol{n} - \cos\theta\mathbf{s}) / \sin\theta$. The tidal torque has two components, one along $\boldsymbol{s}$ that drives the spin rate to synchronous and one along $\boldsymbol{e}$ that changes the obliquity. Taking the spin rate as a constant (i.e., $d\omega/dt = 0$), the tidal torque changes the spin angular momentum by changing only the spin axis unit vector along $\boldsymbol{e}$

$$\begin{aligned}\frac{d\boldsymbol{s}}{dt}_{\text{tid}} &= \frac{1}{C\omega}(\boldsymbol{\tau}_T\cdot\boldsymbol{e})\boldsymbol{e}\\ \frac{d\boldsymbol{s}}{dt}_{\text{tid}} &= T\left(1-\frac{1}{2}\cos\theta\right)(\boldsymbol{n}-\cos\theta\boldsymbol{s})\end{aligned} \tag{12}$$

From Eq. 12, tidal dissipation drives the spin axis toward the orbit normal, which would ultimately result in zero obliquity. With precessional torques (Eq. 8), the equilibrium Cassini state obliquity is nonzero. All sources of dissipation drive the spin axis to an equilibrium state. The above analysis has focused on solid-body tides, and a treatment of torques at the fluid-solid boundary is included in the Supplementary Materials.

Equilibrium spin state with tidal and fluid-solid boundary dissipation

The complete equations of motion for the outer solid spin axis including torques on the permanent figure (ds/dt_{rot}), torques from tides on the whole body (ds/dt_{tid}), and torques from differential rotation at the fluid-solid boundary (ds/dt_{f}) are

$$\frac{d\boldsymbol{s}}{dt} = \frac{d\boldsymbol{s}}{dt}_{\text{rot}} + \frac{d\boldsymbol{s}}{dt}_{\text{tid}} + \frac{d\boldsymbol{s}}{dt}_{\text{f}} \tag{13}$$

Solving for the steady-state spin axis from $\frac{d\boldsymbol{s}}{dt} = 0$, yields

$$\begin{aligned}s_x &= \sin\theta\cos\phi = \left\{\frac{3}{2}\frac{n}{c}\left[(J_2+C_{22})\cos\theta+C_{22}\right]+\dot{\Omega}\cos i\right\}\frac{\sin\theta}{\dot{\Omega}\sin i}\tan\theta\\ s_y &= \sin\theta\sin\phi = \left[T\left(1-\frac{1}{2}\cos\theta\right)\sin\theta+\frac{K}{C_s}\sin\Delta\epsilon\right]\frac{\sin\theta}{\dot{\Omega}\sin i}\\ s_z &= \cos\theta\end{aligned} \tag{14}$$

Dissipation at the fluid-solid boundary is quantified by the factor K/C_s and the angular separation between the fluid and outer solid spin axes is $\Delta\epsilon$ (see the Supplementary Materials). Torques on the satellite's permanent figure dictate the magnitude of s_x compared to s_z, reinforcing the idea that the obliquity is a forced value so that the precessional periods match. Dissipation is the only mechanism contributing to s_y and driving the spin axis off the Cassini plane. Without dissipation, $\phi = 0$ or π, so the equation for s_x simplifies to Eq. 9. Equation 1 for the Cassini plane offset comes from $|\sin\gamma| = |s_y|$ in Eq. 14.

We also derive the Cassini state relation (a non-linear relationship between the obliquity and known parameters) and one for the spin axis azimuth

$$\begin{aligned}(\dot{\Omega}\sin i)^2 = &\left\{\frac{3}{2}\frac{n}{c}\left[(J_2+C_{22})\cos\theta+C_{22}\right]+\dot{\Omega}\cos i\right\}^2\tan^2\theta\\ &+\left[T\left(1-\frac{1}{2}\cos\theta\right)\sin\theta+\frac{K}{C_s}\sin\Delta\epsilon\right]^2\end{aligned} \tag{15}$$

$$\tan\phi = \frac{\left[T\left(1-\frac{1}{2}\cos\theta\right)+\frac{K}{C_s}\frac{\sin\Delta\epsilon}{\sin\theta}\right]\cos\theta}{\frac{3}{2}\frac{n}{c}\left[(J_2+C_{22})\cos\theta+C_{22}\right]+\dot{\Omega}\cos i} \tag{16}$$

We use Eq. 15 when calculating Io's, Europa's, and Ganymede's obliquities in Table 1. Equation 16 is not used in the main text, but we need it to compare our results to that in (*26*). This is done by taking the limit that the spin axis is close to the Cassini plane such that $\Delta\phi$ is small, so we can use $\tan\phi \approx \sin\phi$ and $|\sin\gamma| = |\sin\theta\sin\phi|$ and turn Eq. 16 into

$$|\sin\gamma| \approx \frac{\left[T\left(1-\frac{1}{2}\cos\theta\right)\sin\theta+\frac{K}{C_s}\sin\Delta\epsilon\right]\cos\theta}{\left|\frac{3}{2}\frac{n}{c}\left[(J_2+C_{22})\cos\theta+C_{22}\right]+\dot{\Omega}\cos i\right|} \tag{17}$$

Equation 17 is almost identical to equation 63 in (*26*), differing only by the denominator and by the fact that they only include pressure coupling and not viscous coupling when evaluating $\Delta\varepsilon$. Equation 17 can only be used for the Moon and not Titan, however, because it assumes that $\Delta\phi$ is small ($\Delta\phi = -6.5\times10^{-4}$° for the Moon), whereas for Titan $\Delta\phi = 22$° (Table 1). Another reason why we avoid Eq. 17 for Titan is because there is a mismatch between the $(J_2 + 2C_{22})/c$ derived from Titan's gravity measurements ($\sim1.6\times10^{-4}$) and that derived from its obliquity ($\sim7.9\times10^{-5}$), so we use Eq. 1 over Eq. 17 when solving for γ and take θ as given rather than solving for it.

Supplementary Materials

This PDF file includes:

Supplementary Text
Fig. S1
Table S1
References

REFERENCES AND NOTES

1. G. J. F. MacDonald, Tidal friction. *Rev. Geophys.* **2**, 467–541 (1964).
2. S. J. Peale, P. Cassen, Contribution of tidal dissipation to lunar thermal history. *Icarus* **36**, 245–269 (1978).
3. A. E. H. Love, *A Treatise on the Mathematical Theory of Elasticity* (Cambridge Univ. Press, Cambridge, 4. ed., 1. paperback ed., 1927).
4. L. less, R. A. Jacobson, M. Ducci, D. J. Stevenson, J. I. Lunine, J. W. Armstrong, S. W. Asmar, P. Racioppa, N. J. Rappaport, P. Tortora, The tides of Titan. *Science* **337**, 457–459 (2012).
5. R. S. Park, R. A. Jacobson, L. Gomez Casajus, F. Nimmo, A. I. Ermakov, J. T. Keane, W. B. McKinnon, D. J. Stevenson, R. Akiba, B. Idini, D. R. Buccino, A. Magnanini, M. Parisi, P. Tortora, M. Zannoni, A. Mura, D. Durante, L. less, J. E. P. Connerney, S. M. Levin, S. J. Bolton, Io's tidal response precludes a shallow magma ocean. *Nature*, (2024), 10.1038/s41586-024-08442-5.
6. J. G. Williams, D. H. Boggs, Tides on the Moon: Theory and determination of dissipation. *JGR Planets* **120**, 689–724 (2015).
7. V. Lainey, J.-E. Arlot, Ö. Karatekin, T. Van Hoolst, Strong tidal dissipation in Io and Jupiter from astrometric observations. *Nature* **459**, 957–959 (2009).

8. B. W. Stiles, R. L. Kirk, R. D. Lorenz, S. Hensley, E. Lee, S. J. Ostro, M. D. Allison, P. S. Callahan, Y. Gim, L. Iess, P. P. Del Marmo, G. Hamilton, W. T. K. Johnson, R. D. West, The Cassini Radar Team, Determining Titan's spin state from *Cassini* radar images. *Astron. J* **135**, 1669–1680 (2008).
9. L. Iess, N. J. Rappaport, R. A. Jacobson, P. Racioppa, D. J. Stevenson, P. Tortora, J. W. Armstrong, S. W. Asmar, Gravity field, shape, and moment of inertia of Titan. *Science* **327**, 1367–1369 (2010).
10. D. Durante, D. J. Hemingway, P. Racioppa, L. Iess, D. J. Stevenson, Titan's gravity field and interior structure after Cassini. *Icarus* **326**, 123–132 (2019).
11. V. Lainey, L. G. Casajus, J. Fuller, M. Zannoni, P. Tortora, N. Cooper, C. Murray, D. Modenini, R. S. Park, V. Robert, Q. Zhang, Resonance locking in giant planets indicated by the rapid orbital expansion of Titan. *Nat. Astron.* **4**, 1053–1058 (2020).
12. R. A. Jacobson, The orbits of the main saturnian satellites, the saturnian system gravity field, and the orientation of Saturn's pole. *Astron. J* **164**, 199 (2022).
13. G. Colombo, Cassini's second and third laws. *Astron. J* **71**, 891 (1966).
14. S. J. Peale, Generalized Cassini's Laws. *Astron. J* **74**, 483 (1969).
15. P. Goldreich, S. J. Peale, The obliquity of Venus. *Astron. J* **75**, 273 (1970).
16. S. J. Peale, Possible histories of the obliquity of Mercury. *Astron. J* **79**, 722 (1974).
17. W. R. Ward, Tidal friction and generalized Cassini's laws in the solar system. *Astron. J* **80**, 64 (1975).
18. J. G. Williams, D. H. Boggs, C. F. Yoder, J. T. Ratcliff, J. O. Dickey, Lunar rotational dissipation in solid body and molten core. *J. Geophys. Res.* **106**, 27933–27968 (2001).
19. B. Gladman, D. D. Quinn, P. Nicholson, R. Rand, Synchronous locking of tidally evolving satellites. *Icarus* **122**, 166–192 (1996).
20. C. F. Yoder, The free librations of a dissipative Moon. *Phil. Trans. R. Soc. Lond. Ser. A. Math. Phys. Sci.* **303**, 327–338 (1981).
21. J. O. Dickey, P. L. Bender, J. E. Faller, X. X. Newhall, R. L. Ricklefs, J. G. Ries, P. J. Shelus, C. Veillet, A. L. Whipple, J. R. Wiant, J. G. Williams, C. F. Yoder, Lunar laser ranging: A continuing legacy of the Apollo program. *Science* **265**, 482–490 (1994).
22. J. G. Williams, A. S. Konopliv, D. H. Boggs, R. S. Park, D.-N. Yuan, F. G. Lemoine, S. Goossens, E. Mazarico, F. Nimmo, R. C. Weber, S. W. Asmar, H. J. Melosh, G. A. Neumann, R. J. Phillips, D. E. Smith, S. C. Solomon, M. M. Watkins, M. A. Wieczorek, J. C. Andrews-Hanna, J. W. Head, W. S. Kiefer, I. Matsuyama, P. J. McGovern, G. J. Taylor, M. T. Zuber, Lunar interior properties from the GRAIL mission: Lunar interior properties. *J. Geophys. Res. Planets* **119**, 1546–1578 (2014).
23. R.-M. Baland, T. Van Hoolst, M. Yseboodt, Ö. Karatekin, Titan's obliquity as evidence of a subsurface ocean? *Astron. Astrophys.* **530**, A141 (2011).
24. A. Stark, J. Oberst, F. Preusker, S. J. Peale, J. Margot, R. J. Phillips, G. A. Neumann, D. E. Smith, M. T. Zuber, S. C. Solomon, First MESSENGER orbital observations of Mercury's librations. *Geophys. Res. Lett.* **42**, 7881–7889 (2015).
25. J. L. Margot, S. J. Peale, R. F. Jurgens, M. A. Slade, I. V. Holin, Large longitude libration of mercury reveals a molten core. *Science* **316**, 710–714 (2007).
26. O. Organowski, M. Dumberry, Viscoelastic relaxation within the moon and the phase lead of its Cassini state. *JGR Planets* **125**, e2020JE006386 (2020).
27. P. Goldreich, Precession of the Moon's core. *J. Geophys. Res.* **72**, 3135–3137 (1967).
28. C. Stys, M. Dumberry, The Cassini state of the moon's inner core. *JGR Planets* **123**, 2868–2892 (2018).
29. J. Zhang, M. Dumberry, Viscous dissipation in the fluid core of the moon. *JGR Planets* **126**, e2021JE006966 (2021).
30. R. Meriggiola, L. Iess, W. Bryan, J. Stiles, I. Lunine, G. Mitri, The rotational dynamics of Titan from Cassini RADAR images. *Icarus* **275**, 183–192 (2016).
31. R.-M. Baland, G. Tobie, A. Lefèvre, T. Van Hoolst, Titan's internal structure inferred from its gravity field, shape, and rotation state. *Icarus* **237**, 29–41 (2014).
32. R.-M. Baland, A. Coyette, T. Van Hoolst, Coupling between the spin precession and polar motion of a synchronously rotating satellite: Application to Titan. *Celest. Mech. Dyn. Astr.* **131**, 11 (2019).
33. C. Sagan, S. F. Dermott, The tide in the seas of Titan. *Nature* **300**, 731–733 (1982).
34. F. Sohl, W. D. Sears, R. D. Lorenz, Tidal dissipation on Titan. *Icarus* **115**, 278–294 (1995).
35. E. M. A. Chen, F. Nimmo, G. A. Glatzmaier, Tidal heating in icy satellite oceans. *Icarus* **229**, 11–30 (2014).
36. H. C. F. C. Hay, I. Matsuyama, Nonlinear tidal dissipation in the subsurface oceans of Enceladus and other icy satellites. *Icarus* **319**, 68–85 (2019).
37. B. Idini, F. Nimmo, Resonant stratification in Titan's global ocean. *Planet. Sci. J.* **5**, 15 (2024).
38. J. Wisdom, Spin-orbit secondary resonance dynamics of enceladus. *Astron. J* **128**, 484–491 (2004).
39. R. Fan, L. Zhao, Y. Lu, H. Nie, H. Wei, Impacts of currents and waves on bottom drag coefficient in the east China shelf seas. *J. Geophys. Res. Oceans* **124**, 7344–7354 (2019).
40. R. L. Kirk, D. J. Stevenson, Thermal evolution of a differentiated Ganymede and implications for surface features. *Icarus* **69**, 91–134 (1987).
41. G. Mitri, A. P. Showman, Thermal convection in ice-I shells of Titan and Enceladus. *Icarus* **193**, 387–396 (2008).
42. C. F. Chyba, D. G. Jankowski, P. D. Nicholson, Tidal evolution in the Neptune-Triton system. *Astron. Astrophys.* **219**, L23–L26 (1989).
43. S. J. Peale, P. Cassen, R. T. Reynolds, Tidal dissipation, orbital evolution, and the nature of Saturn's inner satellites. *Icarus* **43**, 65–72 (1980).
44. W. Sears, Tidal dissipation in oceans on Titan. *Icarus* **113**, 39–56 (1995).
45. G. Tobie, A. Mocquet, C. Sotin, Tidal dissipation within large icy satellites: Applications to Europa and Titan. *Icarus* **177**, 534–549 (2005).
46. F. Nimmo, B. G. Bills, Shell thickness variations and the long-wavelength topography of Titan. *Icarus* **208**, 896–904 (2010).
47. C. Béghin, O. Randriamboarison, M. Hamelin, E. Karkoschka, C. Sotin, R. C. Whitten, J.-J. Berthelier, R. Grard, F. Simões, Analytic theory of Titan's Schumann resonance: Constraints on ionospheric conductivity and buried water ocean. *Icarus* **218**, 1028–1042 (2012).
48. G. Tobie, J. I. Lunine, C. Sotin, Episodic outgassing as the origin of atmospheric methane on Titan. *Nature* **440**, 61–64 (2006).
49. S. Goossens, B. Van Noort, A. Mateo, E. Mazarico, W. Van Der Wal, A low-density ocean inside Titan inferred from Cassini data. *Nat. Astron.* **8**, 846–855 (2024).
50. B. Journaux, K. Kalousová, C. Sotin, G. Tobie, S. Vance, J. Saur, O. Bollengier, L. Noack, T. Rückriemen-Bez, T. Van Hoolst, K. M. Soderlund, J. M. Brown, Large ocean worlds with high-pressure ices. *Space Sci. Rev.* **216**, 7 (2020).
51. D. Hemingway, F. Nimmo, H. Zebker, L. Iess, A rigid and weathered ice shell on Titan. *Nature* **500**, 550–552 (2013).
52. K. Lambeck, Effects of tidal dissipation in the oceans on the Moon's orbit and the Earth's rotation. *J. Geophys. Res.* **80**, 2917–2925 (1975).
53. B. G. Bills, G. A. Neumann, D. E. Smith, M. T. Zuber, Improved estimate of tidal dissipation within Mars from MOLA observations of the shadow of Phobos. *J. Geophys. Res. Planets* **110**, E07004 (2005).
54. E. Mazarico, D. Buccino, J. Castillo-Rogez, A. J. Dombard, A. Genova, H. Hussmann, W. S. Kiefer, J. I. Lunine, W. B. McKinnon, F. Nimmo, R. S. Park, J. H. Roberts, D. K. Srinivasan, G. Steinbrügge, P. Tortora, P. Withers, The Europa clipper gravity and radio science investigation. *Space Sci. Rev.* **219**, 30 (2023).
55. J.-L. Margot, S. Padovan, D. Campbell, S. Peale, F. Ghigo, Measurements of the spin states of Europa and Ganymede, in *European Planetary Science Congress* (2013), vol. 45, pp. 504.02.
56. P. Cappuccio, A. Hickey, D. Durante, M. Di Benedetto, L. Iess, F. De Marchi, C. Plainaki, A. Milillo, A. Mura, Ganymede's gravity, tides and rotational state from JUICE's 3GM experiment simulation. *Planet. Space Sci.* **187**, 104902 (2020).
57. P. Cappuccio, M. Di Benedetto, D. Durante, L. Iess, Callisto and europa gravity measurements from JUICE 3GM experiment simulation. *Planet. Sci. J.* **3**, 199 (2022).
58. T. Tokano, T. Van Hoolst, Ö. Karatekin, Polar motion of Titan forced by the atmosphere. *J. Geophys. Res.* **116**, E05002 (2011).
59. A. Coyette, R.-M. Baland, T. Van Hoolst, Variations in rotation rate and polar motion of a non-hydrostatic Titan. *Icarus* **307**, 83–105 (2018).
60. B. G. Bills, F. Nimmo, Forced obliquity and moments of inertia of Titan. *Icarus* **196**, 293–297 (2008).
61. E. Asphaug, A. Reufer, Late origin of the Saturn system. *Icarus* **223**, 544–565 (2013).
62. M. Ćuk, L. Dones, D. Nesvorný, Dynamical evidence for a late formation of Saturn's moons. *Astrophys. J* **820**, 97 (2016).
63. B. G. Bills, F. Nimmo, "How Does Titan Retain a Finite Orbital Eccentricity?" (2004), p. 1341; https://ui.adsabs.harvard.edu/abs/2004LPI....35.1341B.
64. J. Wisdom, R. Dbouk, B. Militzer, W. B. Hubbard, F. Nimmo, B. G. Downey, R. G. French, Loss of a satellite could explain Saturn's obliquity and young rings. *Science* **377**, 1285–1289 (2022).
65. R. M. Canup, Origin of Saturn's rings and inner moons by mass removal from a lost Titan-sized satellite. *Nature* **468**, 943–946 (2010).
66. L. F. A. Teodoro, J. A. Kegerreis, P. R. Estrada, M. Ćuk, V. R. Eke, J. N. Cuzzi, R. J. Massey, T. D. Sandnes, A recent impact origin of Saturn's rings and mid-sized moons. *Astrophys. J* **955**, 137 (2023).
67. P. Tortora, M. Zannoni, F. Nimmo, E. Mazarico, L. Iess, C. Sotin, A. Hayes, M. Malaska, "Titan gravity investigation with the Oceanus mission" (2017), p. 17876; https://ui.adsabs.harvard.edu/abs/2017EGUGA..1917876T.
68. J. W. Barnes, E. P. Turtle, M. G. Trainer, R. D. Lorenz, S. M. MacKenzie, W. B. Brinckerhoff, M. L. Cable, C. M. Ernst, C. Freissinet, K. P. Hand, A. G. Hayes, S. M. Hörst, J. R. Johnson, E. Karkoschka, D. J. Lawrence, A. Le Gall, J. M. Lora, C. P. McKay, R. S. Miller, S. L. Murchie, C. D. Neish, C. E. Newman, J. Núñez, M. P. Panning, A. M. Parsons, P. N. Peplowski, L. C. Quick, J. Radebaugh, S. C. R. Rafkin, H. Shiraishi, J. M. Soderblom, K. S. Sotzen, A. M. Stickle, E. R. Stofan, C. Szopa, T. Tokano, T. Wagner, C. Wilson, R. A. Yingst, K. Zacny, S. C. Stähler, Science goals and objectives for the Dragonfly Titan rotorcraft relocatable lander. *Planet. Sci. J.* **2**, 130 (2021).
69. B. G. Bills, F. Nimmo, Rotational dynamics and internal structure of Titan. *Icarus* **214**, 351–355 (2011).
70. A. C. M. Correia, J. Laskar, The four final rotation states of Venus. *Nature* **411**, 767–770 (2001).
71. A. S. Konopliv, R. S. Park, D. Yuan, S. W. Asmar, M. M. Watkins, J. G. Williams, E. Fahnestock, G. Kruizinga, M. Paik, D. Strekalov, N. Harvey, D. E. Smith, M. T. Zuber, The JPL lunar gravity field to spherical harmonic degree 660 from the GRAIL Primary Mission. *JGR Planets* **118**, 1415–1434 (2013).
72. J. D. Anderson, R. A. Jacobson, E. L. Lau, W. B. Moore, G. Schubert, Io's gravity field and interior structure. *J. Geophys. Res.* **106**, 32963–32969 (2001).

73. L. Gomez Casajus, A. I. Ermakov, M. Zannoni, J. T. Keane, D. Stevenson, D. R. Buccino, D. Durante, M. Parisi, R. S. Park, P. Tortora, S. J. Bolton, gravity field of Ganymede after the *Juno* extended mission. *Geophys. Res. Lett.* **49**, e2022GL099475 (2022).
74. B. Noyelles, Expression of Cassini's third law for Callisto, and theory of its rotation. *Icarus* **202**, 225–239 (2009).
75. A. W. Harris, W. R. Ward, Dynamical constraints on the formation and evolution of planetary bodies. *Annu. Rev. Earth Planet. Sci.* **10**, 61–108 (1982).
76. M. Dumberry, The influence of a fluid core and a solid inner core on the Cassini state of Mercury. *J. Geophys. Res. Oceans* **126**, e2020JE006621 (2021).
77. M. G. Rochester, The secular decrease of obliquity due to dissipative core–mantle coupling. *Geophys. J. Int.* **46**, 109–126 (1976).
78. J. Meyer, J. Wisdom, Precession of the lunar core. *Icarus* **211**, 921–924 (2011).
79. V. Viswanathan, N. Rambaux, A. Fienga, J. Laskar, M. Gastineau, Observational constraint on the radius and oblateness of the lunar core-mantle boundary. *Geophys. Res. Lett.* **46**, 7295–7303 (2019).
80. H. A. Zebker, B. Stiles, S. Hensley, R. Lorenz, R. L. Kirk, J. Lunine, Size and shape of Saturn's moon Titan. *Science* **324**, 921–923 (2009).

Acknowledgments: We are grateful to the reviewers for reviews that made the conclusions of this paper much more robust. We also thank B. Bills, M. Ćuk, and T. Van Hoolst for useful discussions. **Funding:** This material is based upon work supported by the National Science Foundation Graduate Research Fellowship under grant no. DGE-1842400. **Author contributions:** Conceptualization: B.G.D. and F.N. Methodology: B.G.D. and F.N. Investigation: B.G.D. and F.N. Visualization: B.G.D. and F.N. Supervision: F.N. Writing–original draft: B.G.D. and F.N. Writing–review and editing: B.G.D. and F.N. **Competing interests:** The authors declare that they have no competing interests. **Data and materials availability:** All data needed to evaluate the conclusions in the paper are present in the paper and/or the Supplementary Materials. The code used to produce the findings and the figures in the paper is available at the Dryad repository DOI: 10.5061/dryad.cvdncjtcw and at the corresponding author's GitHub repository: https://github.com/bgdowney/Titan_2025.

Submitted 26 March 2024
Accepted 7 January 2025
Published 5 February 2025
10.1126/sciadv.adl4741